

# X-ray Emission Spectroscopy

**Alexander Moewes**  
University of Saskatchewan

## Principal Contacts

Beamline Team Leader	Alexander Moewes University of Saskatchewan moewes@usask.ca
Beamline Development Scientist	Lijun Lu Canadian Light Source Inc. lijun.lu@lightsource.ca

## Beamline Overview

Status	Recommended by the FAC as of December 31, 2001	
Source	Elliptically polarized undulator	
Monochromator	Plane grating	
Energy range	80–2000 eV	
Resolving power ( $E/\Delta E$ )	$\geq 5000$	
Vacuum	$\leq 5 \times 10^{-10}$ mbar	
	First stage (2005)	Second stage (2006)
Flux (photons/s/100 mA):		
Maximum for $E/\Delta E = 5000$	$\geq 2 \times 10^{13}$	$\geq 8 \times 10^{13}$
At 100 eV for $E/\Delta E = 5000$	$\geq 2 \times 10^{13}$	$\geq 8 \times 10^{13}$
At 1000 eV for $E/\Delta E = 2000$	$5 \times 10^{12}$	$2 \times 10^{11}$
Spot size	$\sim 50 \times 50 \mu\text{m}$	$\leq 10 \times 10 \mu\text{m}$
Stability of spot	$\leq 10 \mu\text{m}$	$\sim 1 \mu\text{m}$

The X-ray emission spectroscopy (XES) beamline will be designed to provide high flux and moderate resolution for applications in soft X-ray spectroscopy. Excitation energies will be provided over a wide energy range (80–2000 eV); the two endstations will allow for resonant soft X-ray emission spectroscopy (XES), resonant elastic X-ray scattering (REXS) and soft X-ray absorption spectroscopy (XAS).

## Science

*Magnetic materials.* The ultimate goal in magnetic materials research is to increase recording density. Towards this end, the XES beamline will be used for the study of electronic structures of antiferromagnetic 3d-transition-metal monoxides, metal fluorides, ferromagnetic multilayer films, and the magnetic-coupling effects in cobalt-platinum multi-layered thin films.

*Correlated electron materials.* The electronic properties of complex materials containing 3d, 5d and 4f elements are of fundamental interest, because the wave functions of these elements hybridize with other elements (such as carbon and oxygen) to produce subtle coupling of electrical, magnetic and elastic properties. These interactions give rise to useful piezoelectric, electrostrictive, magnetostrictive and giant magnetoresistance effects that lead to device-oriented applications.

*Nanoparticles.* Due to their small size, nanoparticles often exhibit electronic properties that differ from the properties of the corresponding bulk material. Research in this area is motivated by the possibility of designing materials with novel electronic, optical, magnetic, photochemical and catalytic properties. Silicon and diamond nanoparticles may find applications in thin film techniques and in microelectronic devices.

## Beamline Team Research Activities

### Band structure of $\text{MgB}_2$ and graphite from resonant inelastic X-ray scattering

A. Moewes<sup>1</sup>, J. Kortus<sup>2</sup> and E. Z. Kurmaev<sup>3</sup>

<sup>1</sup>University of Saskatchewan

<sup>2</sup>MPI für Festkörperforschung, Stuttgart, Germany

<sup>3</sup>Institute of Metal Physics, Russian Academy of Sciences-Ural Division, Russia

The recent discovery of superconductivity in  $\text{MgB}_2$  up to an unexpectedly high transition temperature of 39 K [1] has stimulated extensive scientific interest in this material and its possible applications. The reported values for  $2\Delta/k_B T_C$  of 1.2 to 4 from tunneling measurements [2] and the analysis of the temperature and magnetic field dependences of the specific heat [3] suggest anisotropic or multiple superconducting gaps. Experimental evidence [4] now supports a multiband

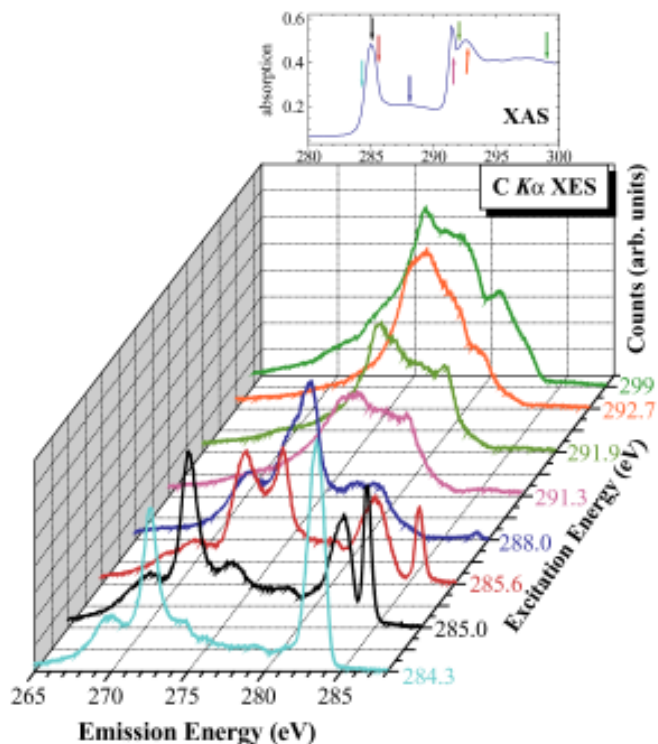


Figure 14-1 X-ray emission spectra of HOPG vs. excitation energy near the carbon 1s threshold excitation. The arrows in the absorption spectrum (XAS) of the inset figure indicate the excitation energies at which the emission spectra were taken.

model, because spectroscopy experiments clearly show the existence of two distinct superconducting gaps that coexist up to  $T_c$ . This would place  $\text{MgB}_2$  in a unique class of superconductors where different parts of the Fermi surface with 2-D and 3-D character contribute to superconductivity. This interesting new behaviour arises from the particular shape of the Fermi surface in  $\text{MgB}_2$  [5]. We have shown that there is good agreement between the calculations and the electronic structure obtained from resonant inelastic X-ray scattering (RIXS) on polycrystalline  $\text{MgB}_2$  samples, suggesting that electron-electron interactions are not important.

The standard experimental tool for this task would be angle-resolved photoelectron spectroscopy (ARPES), which measures the energy of the emitted photoelectrons and their direction with respect to the crystallographic axis. However, ARPES measurements can be realized only on single crystals. First reports of successful growth of single crystals have appeared recently, but thus far no reports on ARPES measurements of  $\text{MgB}_2$  are available.

Due to the different processes and their underlying

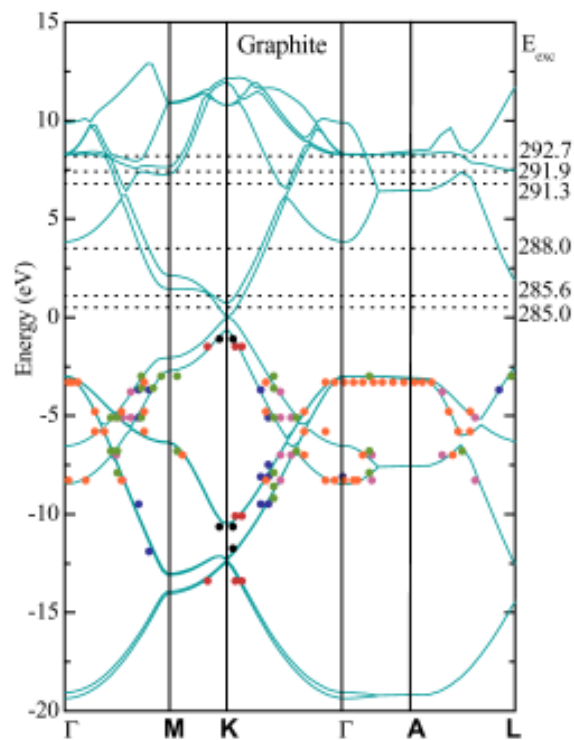


Figure 14-2 Band mapping of graphite using resonant inelastic X-ray scattering. The lines are the calculated band structures and the dots are the experimental results.

selection rules, RIXS provides information that is truly complementary to the well-established ARPES. RIXS can be applied to many materials that are difficult or impossible to study by ARPES, such as insulators and polycrystalline materials. The main drawback of RIXS is that the  $\mathbf{k}$ -selectivity is given indirectly via the dispersion of the unoccupied bands. The vector  $\mathbf{k}$  can be determined unambiguously from the X-ray experiments only for high symmetry points and band edges.

The traditional approach for band mapping using RIXS starts with recording near-threshold X-ray absorption spectra in order to map the unoccupied states. However, it is generally difficult to determine the energy positions of important features due to core-hole effects in absorption. We suggest starting the procedure by measuring the core-level binding energy ( $E_{be}$ ) and locating it with respect to the Fermi level of the band structure calculation. It is then possible to select the important excitation energies ( $E_{exc}$ ) from the calculated dispersion curves for unoccupied states.  $E_{exc}$  is subsequently estimated with respect to this zero position ( $E_{exc} - E_{be}$ ).

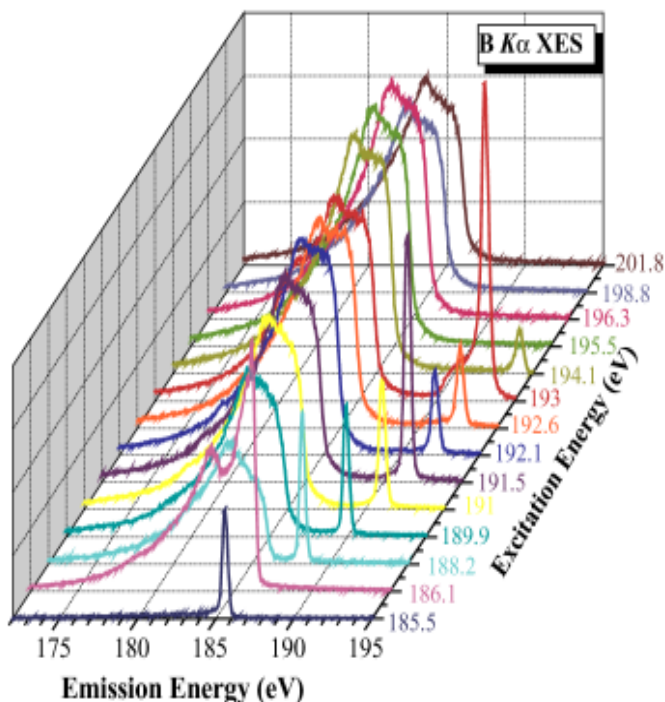


Figure 14-3 Energy-dependent X-ray emission spectra of  $MgB_2$  near the boron  $1s$  threshold excitation.

In order to map the band dispersion, one must be able to select  $k$ -values in the Brillouin zone. This criterion can be fulfilled when tuning the excitation energy near the core-level absorption threshold (and the core electrons are excited to unoccupied states just above the Fermi level). The measured X-ray emission spectra show a strong dependence on  $E_{exc}$ ; this is thought to be due to an absorption-emission process that occurs as a single scattering event with crystal-momentum conservation. Thus, when a core electron is promoted to the conduction band with a crystal momentum that depends on the incident photon energy, an emission from the valence band at the same place in the Brillouin zone will be induced. The coherence between absorption and emission is a consequence of the fast decay process, while the momentum conservation is due to delocalization of the electron-hole pair of the final state.

Soft X-ray fluorescence measurements of polycrystalline  $MgB_2$  and highly oriented pyrolytic graphite (HOPG) were performed using the soft X-ray fluorescence endstation on Beamline 8.0.1 at the ALS [6]. The correlation of the X-ray emission spectra with excitation

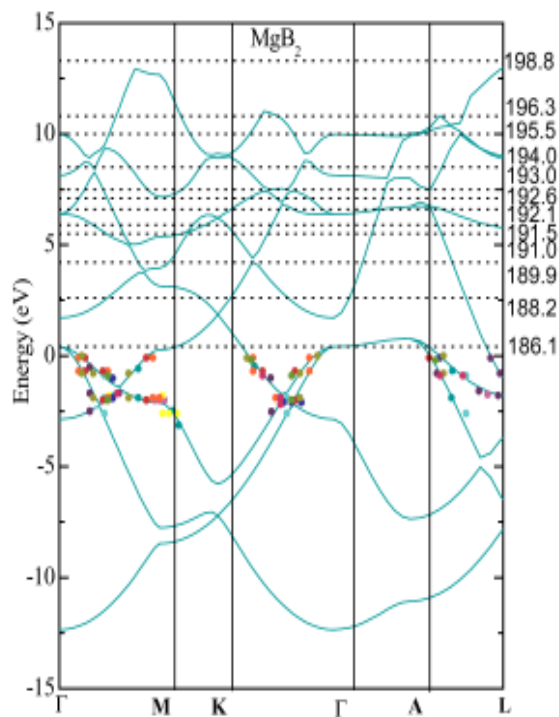


Figure 14-4 Band mapping of  $MgB_2$  using resonant inelastic X-ray scattering. The lines are the calculated band structures and the dots are the experimental results.

energy for HOPG (Figure 14-1) was in good agreement with previous experimental data [7] on this system. Only the inelastic part of each emission spectrum was taken into account for the band mapping procedure. The possible unoccupied states populated during the absorption were determined by intersecting the excitation energies (the dotted horizontal lines in Figure 14-2) and the calculated dispersion curves for the unoccupied states. Due to  $k$ -conservation, the participating occupied states from which the X-ray transition occurs are located vertically below the unoccupied states in the occupied bands. They can be traced from features of the measured X-ray emission spectra at selected excitation energy (see Figure 14-1). The band structure value  $E_{map}$  of these features is also determined on the binding energy scale. The colours of the experimental points displayed in the bands in Figures 14-2 and 14-4 correspond to the colours of the emission spectra in Figures 14-1 and 14-3. These experimental points should lie close to the calculated dispersion curves for occupied states if the experimental and theoretical electronic structures agree. This procedure was carried out for all values of  $E_{exc}$ .

Using the X-ray emission spectra of Figure 14·1 and the carbon 1s binding energy of graphite ( $E = 284.5$  eV) together with the procedure described above, we performed quantitative RIXS band mapping for graphite. The experimental points were shown to fit well with the band structure calculations. After reproducing the well-understood electronic structure of graphite, our group focused on  $\text{MgB}_2$ .

Using the measured boron X-ray emission spectra displayed in Figure 14·3, the boron 1s binding energy in  $\text{MgB}_2$  ( $E = 185.5$  eV) and the same procedure, we mapped out the bands for  $\text{MgB}_2$  (Figure 14·4). A reasonably good agreement between our experimental results and the theoretical band structure was found.

It should be noted that the states in the vicinity of the Fermi level have a strong local boron p-character, supporting the main conclusion of all the present band structure calculations: the boron 2p states are responsible for the superconductivity in  $\text{MgB}_2$ . The dispersion of the important  $\sigma$ -bands in the  $\Gamma$ -K and  $\Gamma$ -M directions is well reproduced. The overall good agreement between theory and experiment suggests that electron-electron interactions are not important (beyond the mean-field treatment of these correlations within density functional theory), and that  $\text{MgB}_2$  behaves like a conventional metal that is well described by band theory. This has important implications for the interpretation of current experimental results. It seems rather unlikely that in this case a large Coulomb pseudopotential  $\mu^*$  is the reason for the observed reduced total isotope effect [8]. Other explanations such as anharmonicity or non-linear electron-phonon coupling have yet to be explored. Optical spectroscopy is also a direct probe of the electronic structure, but the reported plasma frequency of about 1.5 eV is in utter disagreement with the plasma frequency of 7 eV calculated from the band structure. It would be tempting to ascribe this discrepancy to correlation effects, so that the missing spectral weight would be shifted to some incoherent excitations. Our results lend credibility to optical properties calculated from the band structure, while interband conductivity and other mechanisms have yet to be investigated in order to explain this discrepancy.  $\text{MgB}_2$  seems to be described best by the conventional methods. Despite its simple structure, it shows very complex behaviour, and has not revealed all its secrets yet.

The synchrotron data sets for this work were collected at the ALS. This work was supported by NSERC, the Russian State Program on Superconductivity, and a NATO Collaborative Linkage Grant. ✨

## References

- [1] J. Nagamatsu et al. *Nature* **2001**, *410*, 63.
- [2] G. Karapetrov et al. *Phys. Rev. Lett.* **2001**, *86*, 4374.
- [3] F. Bouquet et al. *Phys. Rev. Lett.* **2001**, *87*, 047001.
- [4] A. Y. Liu et al. *Phys. Rev. Lett.* **2001**, *87*, 087005.
- [5] J. Kortus et al. *Phys. Rev. Lett.* **2001**, *86*, 4656.
- [6] J. J. Jia et al. *Rev. Sci. Instrum.* **1995**, *66*, 1394.
- [7] J. A. Carlisle et al. *Phys. Rev. Lett.* **1995**, *74*, 1234.
- [8] D. G. Hinks et al. *Nature* **2001**, *411*, 457.

Table 14·1 XES beamline team

Bonn University, Germany	H. Modrow
Canadian Light Source	Emil Hallin Lijun Lu
Institute of Metal Physics, Russia	E. Z. Kurmaev
Steeacie Institute for Molecular Sciences (NRC)	John S. Tse
Osaka University, Japan	S. Imada S. Suga
Tulane University, USA	D. L. Ederer
University of Alberta	Ronald G. Cavell
University of British Columbia	George Sawatzky Tom Tiedje
University of Saskatchewan	A. Hirose Alexander Moewes (PI) C. Xiao C. E. J. Mitchell H. B. Kraatz J. S. Lee R. Sammynaiken Stephen G. Urquhart
University of Tennessee at Knoxville, USA	T. A. Callcot
University of Western Ontario	T. K. Sham
Uppsala University, Sweden	J. Nordgren
Yonsei University, Korea	C. N. Whang S. Chang

Table 14·2 XES milestones for 2000–2001

Spring, 2001	Letter of intent accepted
Spring, 2001	NSERC funding (Moewes)
Fall, 2001	Design process started
December, 2001	XES Endstation funded (CFI)
February, 2002	Conceptual design report submitted